Received: 24 October 2023 | Revised: 20 December 2023 | Accepted: 7 February 2024

DOI: 10.1002/eng2.12867

RESEARCH ARTICLE

Engineering Reports Open Access WILEY

Electro-thermo-mechanical characterization of shape memory alloy wires for actuator and sensor applications—Part 1: The effects of training

Dominik Scholtes[1,2] | **Stefan Seelecke**[1,2] | **Paul Motzki**[1,2]

[1]Intelligent Materials Systems Lab, Center for Mechatrinics and Automation Technology - ZeMA gGmbH, Saarbrücken, Germany

[2]Intelligent Materials Systems Lab, Department of Systems Engineering, Department of Material Science and Engineering, Saarland University, Saarbrücken, Germany

Correspondence
Dominik Scholtes, Intelligent Materials Systems Lab, Center for Mechatrinics and Automation Technology - ZeMA gGmbH, Saarbrücken 66121, Germany.
Email: dominik.scholtes@imsl.uni-saarland.de

Abstract

So far shape memory alloys (SMA) are mostly characterized by their thermo-mechanical behavior due to the underlying thermal effect. In technical applications however, where their benefits like low weight and compact design become relevant, they are activated electrically. This work presents methods for a thorough and systematic characterization of SMA wire samples under Joule heating with the focus on aspects relevant for applications. The goal is to achieve a precise understanding of the sensor and actuator properties of SMA wire samples with different trainings under varying loads. All experiments are conducted on a custom designed test bench with a commercially available NiTi wire with 72 µm diameter, which enables the direct comparisons of tensile tests to actuation tests. The characterization consists of tensile tests and actuator tests with varying load and heating power for differently trained wire samples. The results vividly represent the influence of heating power, training and changing loads on stroke output, working point and the functional stability of SMA actuator wires. Especially, the evolution of the resistance signal and the influence of the R-phase on self-sensing is discussed. The proposed method enables to compare and choose the best suitable alloy with a fitting training for a desired application.

KEYWORDS

hysteresis, NiTi, resistance, R-phase, self-sensing, shakedown, two-way-effect

1 | INTRODUCTION

Shape Memory Alloy (SMA) wires hold remarkable promise in actuator and sensor applications owing to their unique electro-mechanical properties. These materials exhibit the ability to return to a predetermined shape after deformation when subjected to certain stimuli, such as temperature variations or mechanical stress. Their extraordinary characteristics, including high energy density and self-sensing capabilities, have positioned them as important components in various engineering fields.

However, despite their potential, the comprehensive understanding of SMA wire behavior remains an ongoing challenge. The existing knowledge gaps concern the complicated electro-thermo-mechanical interactions that determine their

functionality, particularly in terms of their performance under varying loads and environmental conditions. Addressing these gaps is crucial to using the full potential of SMA wires in actuation and sensing, ensuring their reliability and optimizing their functionality in diverse applications.

This work has two main objectives: The presentation of a method for the thorough characterization of Joule heated SMA wires from application perspective and using this method to evaluate the effects of training on the actuator and sensor characteristics of SMA wires. The method includes tensile tests as well as a row of actuation experiments and their interpretation. With the results, a statement for the SMA's functional stability, the stroke output as well as the sensor characteristics for various loads is made.

The foundational aspects of SMA (Shape Memory Alloys) have been extensively discussed in scientific literature over recent decades.[1–5] Hence, the following section offers a concise overview of the pertinent elements relevant to this study.

SMAs boast the highest known energy density among actuators and uniquely integrate resistance-based self-sensing capabilities.[6–8] Commonly found in the form of commercially available wires, typically composed of binary Nickel-Titanium (NiTi), these alloys, also known as Nitinol, were first explored by researchers at the U.S. Naval Ordinance Laboratory in 1963.[9] Exhibiting varied thermo-mechanical behavior contingent upon the alloy composition, these materials possess highly hysteric thermal and mechanical characteristics. NiTi with higher nickel content demonstrates superelasticity at room temperature, capable of being stretched up to 10% without sustaining permanent damage.[10] Conversely, the titanium-rich variant undergoes (quasi-)plastic deformation when stretched at room temperature but regains its original geometry upon heating to the transformation temperature—a phenomenon known as the shape memory effect (SME), allowing for the complete recovery of strains of 5% and more.[3] Both effects—superelasticity and SME—are rooted in a reversible rearrangement of the crystal lattice structure of the materials, involving a phase transformation from martensite to austenite and vice versa, where the lattice structure is contingent upon temperature and material stress.[11] Cooling down from austenite can lead to the emergence of a third intermediate phase called the R-Phase, intensifying the material's hysteresis in resistivity.[12,13] SMA wires, typically consisting of titanium-rich NiTi, are commonly activated by either electrical power through Joule heating or passively through contact with a high-temperature fluid.[14,15] Their exceptional energy density renders SMA wires particularly suitable for compact and lightweight actuator systems, such as valves, small-scale gripping systems, and optical image stabilization (OIS).[16–18] Ongoing research delves into fields like continuum robots for catheters and endoscopes, as well as bionic applications.[19–22] In these applications, the inherent self-sensing capability of SMA wires eliminates the need for external position sensors, relying instead on the electrical resistance changes observed during the austenite-martensite transformation. This resistance alteration is contingent upon the contemporary crystal lattice, wire dimensions, and temperature.[14,23]

Basic material characterization of SMA is usually done with differential scanning calorimetry (DSC), temperature controlled tensile tests or thermally-induced phase transformation under a constant stress, which is extensively done by Churchill, Iadicola and Shaw as well as Miller and Lagoudas among others.[4,24–26] Research is also presented on the thermal characteristics of the electrical resistance of Niti.[27–29] What most published data on SMA characterization has in common, is that the temperature of the specimen is controlled by a medium in contact with the wire, so that the temperature of the SMA is known. In contrast to that, the exact wire temperature is an unknown variable in real world applications. In the field of electrically heated SMA, Lewis et al. examined Joule heated wires under convective cooling, while Furst et al. studied the behavior and self-sensing capabilities of antagonistic Joule heated NiTi wires.[14,30] This work complements previous research by presenting the following topics:

- An application-oriented method for the systematic characterization of SMA wires by Joule heating.
- The direct comparison between the tensile behavior and the actuator sensor characteristics under varying loads.
- The examination of the effects of two fundamental training methods on the mechanical and electrical properties.

Using wires as actuators has many benefits compared to other forms like strips or springs. Their flexibility allows for accommodation in tight spatial conditions, they can be bundled to scale the force with consistent dynamics, and they can easily be mounted and electrically connected.[31] SMA wires react to an increase in electrical current respectively temperature in matter of milliseconds.[31] Because of the fast cooling rate and thus possible dynamics of 1 Hz to 10 Hz and even up to 35 Hz, microwires (diameter smaller than 100 µm) have become essential in SMA driven products like OIS and valve systems.[16,32–34] Therefore, this work is based on a commercially available NiTi wire with a diameter of 72 µm. The custom designed test rig used for the experiments, is presented in[35] by Scholtes et al. It features a stress-controlled

installation system for wire insertion directly from the reel without manual handling or cutting. The setup is designed to perform tensile tests as well as actuator tests with free to choose constant loads or springs on the same sample. For the experiments presented in this article, three differently trained wires are examined: as conditioned by the manufacturer, additional thermo-electrical training and additional mechanical training. The training of the SMA is also conducted on the test rig.

A commonly known limit for the application of SMA wire actuators is the ambient temperature. It is set by the transformation temperatures of the alloy, which lies typically at 80–90°C. It can be tuned for example by prestressing the wire and thus increasing the phase transformation temperatures.[36,37] In "Part 2" of this research project, the actuator and sensor characteristics of Joule heated SMA wires in high ambient temperatures are examined. The impact of training and pre-stress on the shift of maximum operating temperature is investigated.

The subsequent sections of this paper are organized in the following manner: The experimental setup, the materials and measurement methods are described in Section 2. In Section 3 follows the presentation of the training procedures and their evaluation. In the subsections of 3, each of the differently treated samples is characterized by tensile tests and actuator tests with various constant loads and springs. The manuscript closes in Section 4 with a conclusion including a summary of the results and an outlook.

2 | EXPERIMENTAL SETUP, MATERIALS AND METHODS

All experiments discussed in the following are conducted on one setup, of which the design, implementation and validation is described exhaustively by Scholtes et al.[35] Refer to that publication for all details on the experiments and the test setup, which are not found in the following brief descriptions.

The test rig, displayed in Figure 1, consists of two clamps mounted on air bearings, that mechanically fix and electrically connect the SMA wire. One clamp is fixed to a load cell, while the opposing one is mounted on a linear drive. The clamps, as well as the wire sample, are positioned inside an isolating chamber to prevent ambient airflow from interfering with the measurements. The temperature inside the chamber is monitored with PT100 temperature sensors and can be controlled. An additional motor is accessible for directly extracting the wire from the reel and securely affixing it to the clamps in a stress-controlled manner. Herewith, after a swap of the SMA sample, repeatable measurement results are ensured. The test rig is multifunctional, which means that it is designed to conduct tensile tests, actuator tests and cyclic tests for shakedown experiments or training. All tests can be run on a single sample, without any further manual intervention, only by switching the software. This key feature enables the direct and precise comparison of the results of actuator tests and tensile tests, as they are performed in the exact same specimen. While the linear drive is run in position-control mode for the tensile tests, it is run in a closed-loop force-control mode for the actuator tests, where arbitrary loads can be mapped.

In general, all tests are run with a Joule heated wire, while it is possible to control either the electrical current or the electrical power. The isolating chamber is also temperature-controlled, but in this paper all experiments are run at room temperature of 23°C. It is designed to enable tests under high constant ambient temperatures but is not made to gradually cool or heat the air inside the chamber. The parameters electrical power or current, maximum strain and strain rate are adjustable for tensile tests. The force values are obtained by the loadcell, on which is the SMA wire is attached via a clamp mounted on an air bearing. The strain of the wire is measured by using the internal encoder of the linear drive. Actuator tests can be performed with an adjustable constant load or an arbitrary linear spring rate with settable pre-stress. Furthermore, the maximum heating current and the heating cycle time are configurable. The electrical supply for heating the SMA wire is provided by a custom designed constant current source with adjustable output currents of 0 mA to 250 mA and up to 24 V. A measurement error of only 10 µA allows, in combination with the measurement of the voltage drop over the wire, a precise resistance measurement also at low currents of 5–10 mA. The whole setup is controlled, and all data is acquired with a "National Instruments" FPGA based system and "NI LabVIEW". An extensive discussion of the design of the test rig, the data acquisition, control and the conduct of experiments is given by Scholtes et al.[35]

For all experiments in this work a "Dynalloy Flexinol HT" NiTi wire with a measured diameter d_0 of 72 µm (in twinned martensite) is used.[37] The initial wire length L_0 is always set to 100 mm in full austenite. For all following results, the wire strain ε is calculated with:

$$\varepsilon = \frac{L - L_0}{L_0} \tag{1}$$

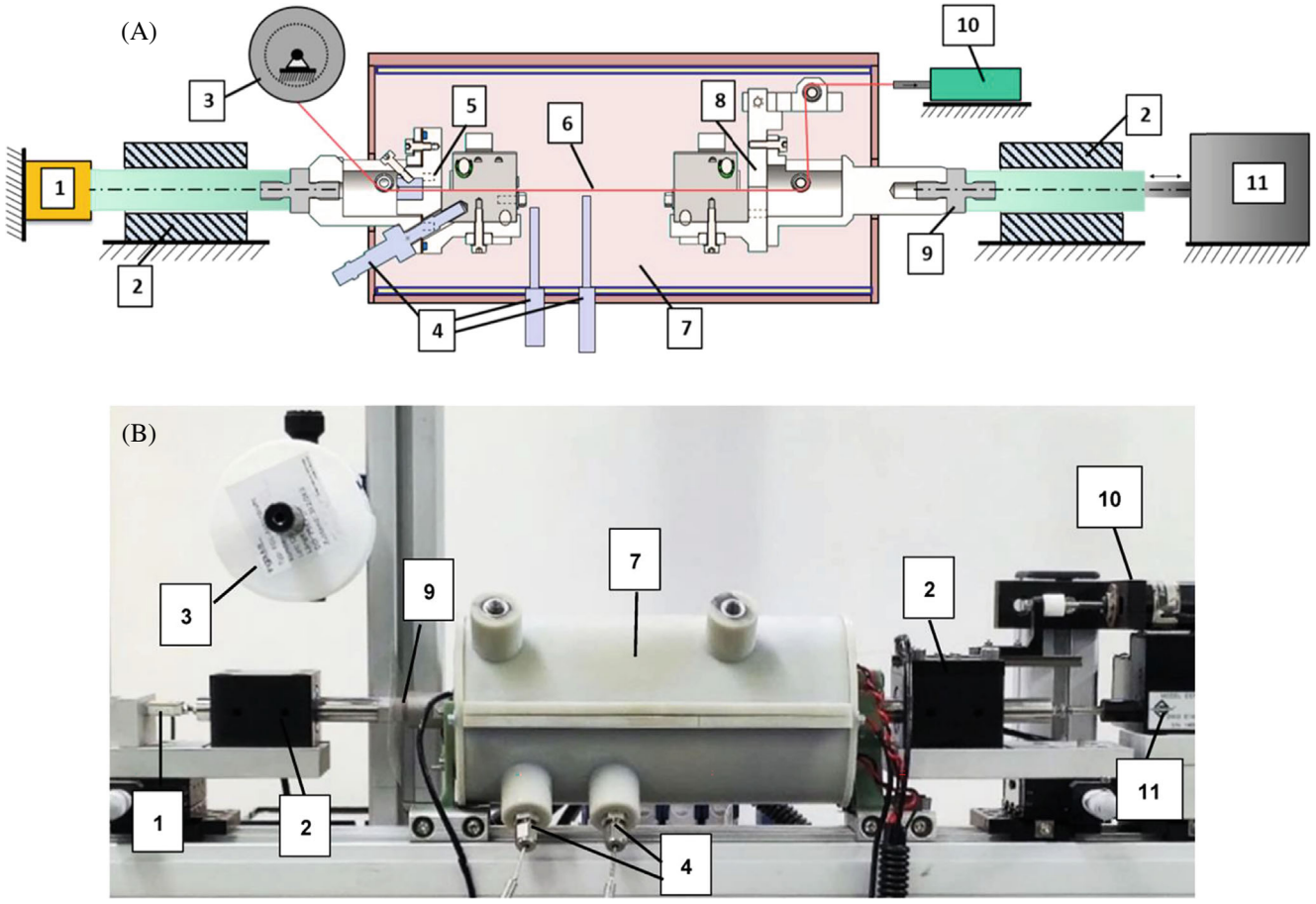

FIGURE 1 (A) Schematic design of the experimental setup. (B) Picture of the fully implemented test rig with closed heating chamber including the following components: 1: load cell; 2: air bearing; 3: SMA wire reel; 4: PT100 sensors; 5: fixed wire clamp; 6: SMA wire; 7: heating chamber; 8: moving wire clamp; 9: insulation adapter; 10: pre-stressing motor; 11: linear direct drive. (Reproduced under terms of the CC-BY license Copyright 2023, Scholtes et al., published by MDPI.)[35]

The engineering stress σ is calculated with

$$\sigma = \frac{F}{A_0} \tag{2}$$

where F is the measured force and A_0 is the initial cross-sectional area of the wire at the length L_0, which is calculated by

$$A_0 = \frac{\pi}{4} \times d_0^2. \tag{3}$$

For a better comparability, no absolute values for stroke or force are discussed. Also, if not described otherwise, a reset procedure is run on the NiTi wire before each experiment. For that, the wire is slack, heated to full austenite and cooled down under these stress-free conditions. This measure ensures that the wire is in the same initial state before every test.

3 | EXPERIMENTS AND RESULTS

The presented characterization method is used to examine the effects of different trainings on the actuator and sensor characteristics, as well as the basic material properties of NiTi wires. The "Dynalloy" wire comes conditioned and ready-to-use. It exhibits a stable material behavior at stresses of up to about 200 MPa, which is typical for commercially

available SMA actuator wires.[36–38] This "as delivered" state of the wire is characterized as reference. With stress limited to 200 MPa, SMA actuators usually exhibit a good fatigue life, but there are some drawbacks. To achieve higher forces the installation space increases, because wire bundles or a transmission stage combined with longer wires are needed. A higher material stress results in a more compact and lightweight system with higher force output and can be used if a shorter lifecycle is acceptable. Therefore, the goal of this research is to achieve a stable stroke and resistance characteristics of the SMA wire at up to 400 MPa of material stress with additional training. It is expected that the thermal, mechanical and electrical characteristics of the SMA actuator wire change and loads above 200 MPa. A residual strain and a shift in working point are the most pronounced effects that are anticipated. Two different trainings are conducted on separate samples. In one method, the wire is thermally cycled, while a constant stress of 400 MPa is applied until it reaches a stable condition once more. The temperature is controlled with a triangular current signal run through the wire. The triangular current signal provides a varied and continuous input, allowing for a more comprehensive analysis of the SMA wire's response across a range of stimuli compared to a square wave for example. It helps to understand the wire's response under changing current levels, especially concerning stress, strain and resistance. The second method is a mechanical training, where the wire is activated by a constant electrical power and is repeatedly stretched with a constant strain rate of 0.01 s^{-1} to 5.5% strain until the residual strain no longer increases.

All three specimen then undergo a so called "basic characterization", which consists of a set of five tensile tests with varying heating power and a certain strain. To paint the whole picture, two more tensile tests are added, where the NiTi wire is pulled in full austenite as well as full detwinned martensite up to 400 MPa. The results allow to extract many important material parameters and perform a first comparison of the training methods. To evaluate the actuator-sensor properties and validate the functional stability, four different actuator tests are performed with each sample: two sets with a constant load of 200 and 400 MPa as well as two sets with spring loads ranging from 100 to 200 MPa and 200 to 400 MPa. These loads are chosen due to their relevance for applications. With up to 200 MPa of stress it is possible to achieve more than one million activation cycles, while up to 400 MPa still enables an acceptable lifetime of the actuator-sensor system with a doubled force output.[36] Comparing spring loads of varying stiffnesses to constant loads, helps to grasp the influence of the slope of a load and enable inter-and extrapolation. The characteristics of loads significantly different than discussed in this paper need to be examined separately, which can be done with the methods introduced in this work.

The order in which the results are discussed does not correspond to the order in which the measurements are carried out. Also, they are not necessarily run on the exact same piece of NiTi material. Depending on the loads that the wire has to endure, a new sample is installed in the test rig and trained accordingly once again for the following experiments.

3.1 | Thermal training

In this subsection, the execution and results of the (electro-)thermal training procedure are discussed. The NiTi wire is loaded with 400 MPa of constant stress. A maximum current of 180 mA with a triangular signal shape and 40 s cycle time is run through the wire to heat it. The current does not fall below a threshold value of 10 mA to ensure a consistent resistance measurement. In Figure 2 the timings of current, voltage, electrical power, strain, stress and resistance are displayed for the first ten cycles of the training procedure. The training procedures shown here are also known as shakedown response.[28,29,39] Especially in the first ten cycles, the typical ratcheting and plastic shakedown behavior for martensite-austenite transformation of NiTi is observed in the strain and the resistance data in Figure 2.

For all 100 cycles, the same ratcheting and plastic shakedown is displayed in Figure 3 in the strain versus power graph. "Ratcheting" describes the movement of the working range in positive strain direction. The maximum martensitic strain of the wire increases about 0.73% from 6.93% (1st cycle in Figure 3) to 7.65% (return point of the last cycle in Figure 3). This plastic shakedown can be seen in Figure 4 on the left. With 2.18% (from 1.08% to 3.26%), the increase of minimum strain in austenite is greater the change in martensite strain. The reason for these observations lies in microstructural changes within the SMA wire, induced by the repeated heating and cooling under load. This causes changed in the arrangement of the crystal lattice and leads to altered stress–strain curves, residual strain and changing transformation temperatures.

Here it should be noted, that due to the reset procedure before the experiment, the characteristics of the first actuation cycle always deviates from the rest of the results with a lower starting strain in martensite. As the wire is cooled down with

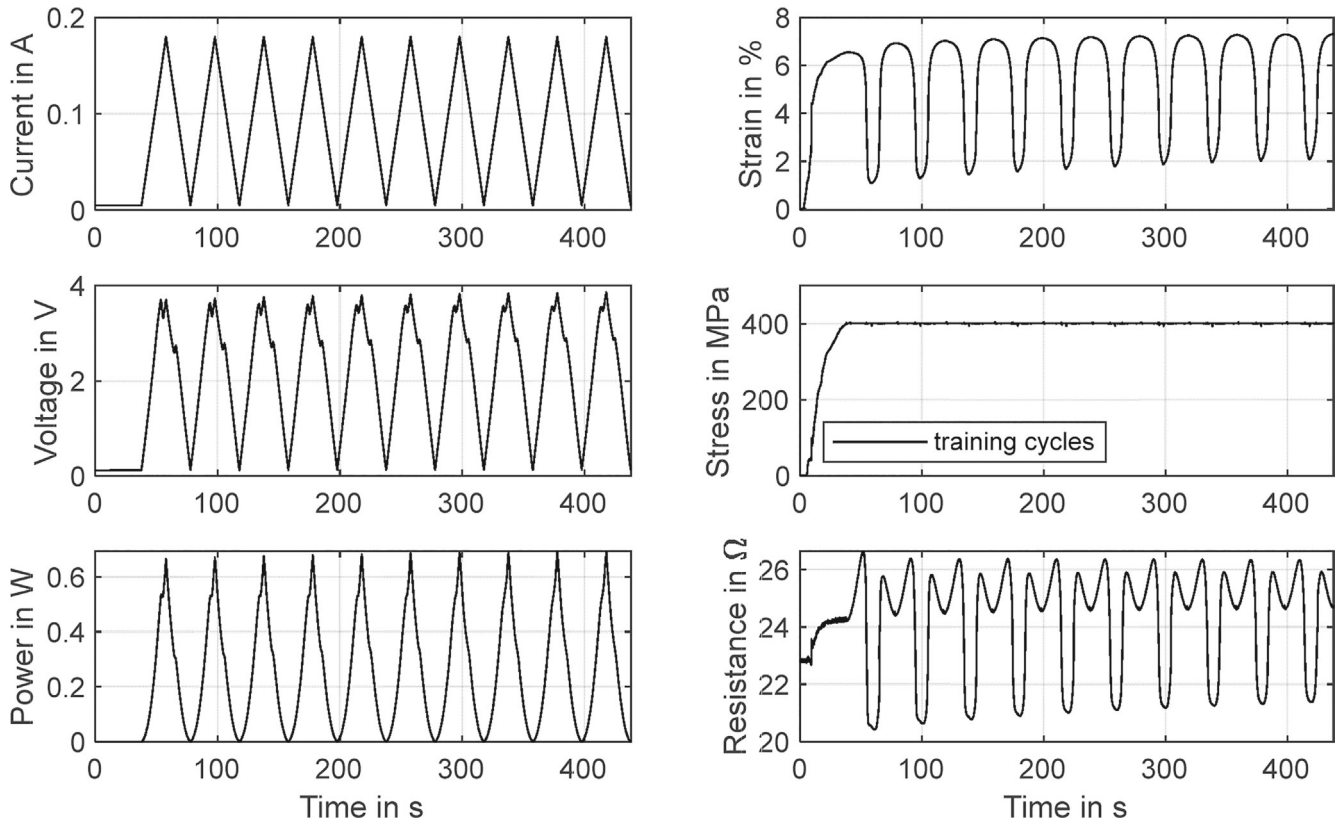

FIGURE 2 Measurement data of the first ten cycles of the thermal training plotted over time. Presented are the triangular activation current signal with an amplitude of 180 mA and a cycle time of 40 s as well as the resulting values of voltage, power, strain and resistance. The stress is held constant at 400 MPa.

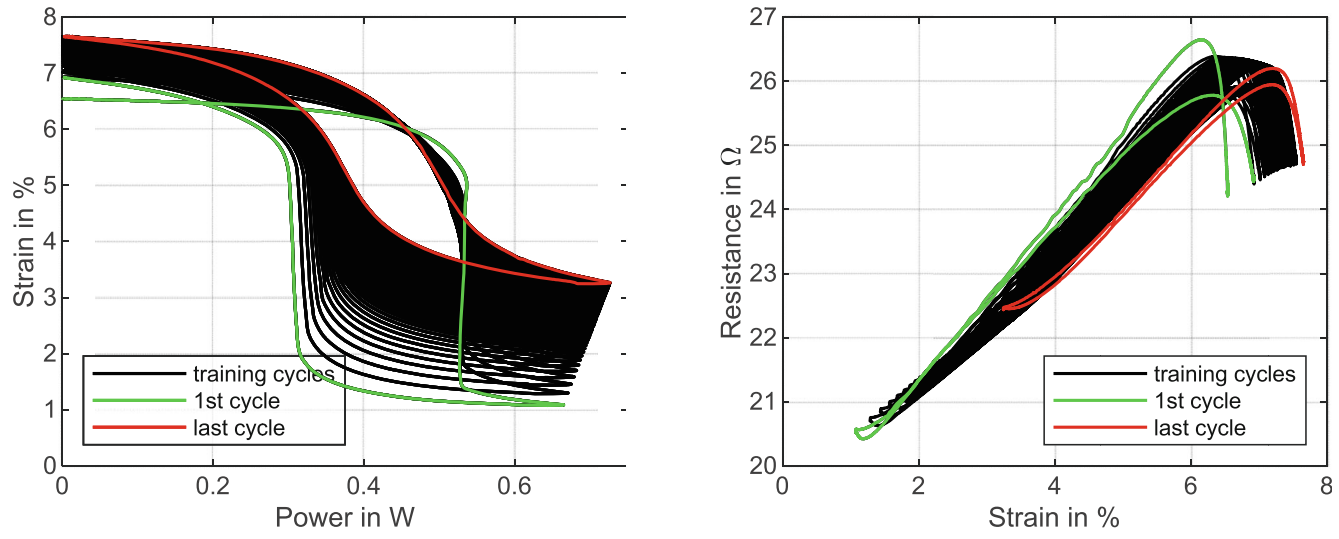

FIGURE 3 Results of the Joule heated thermal training experiment with 100 activation cycles. Illustrated are the evolution of strain versus power (left) and electrical resistance versus strain (right) with first and last cycle highlighted in color.

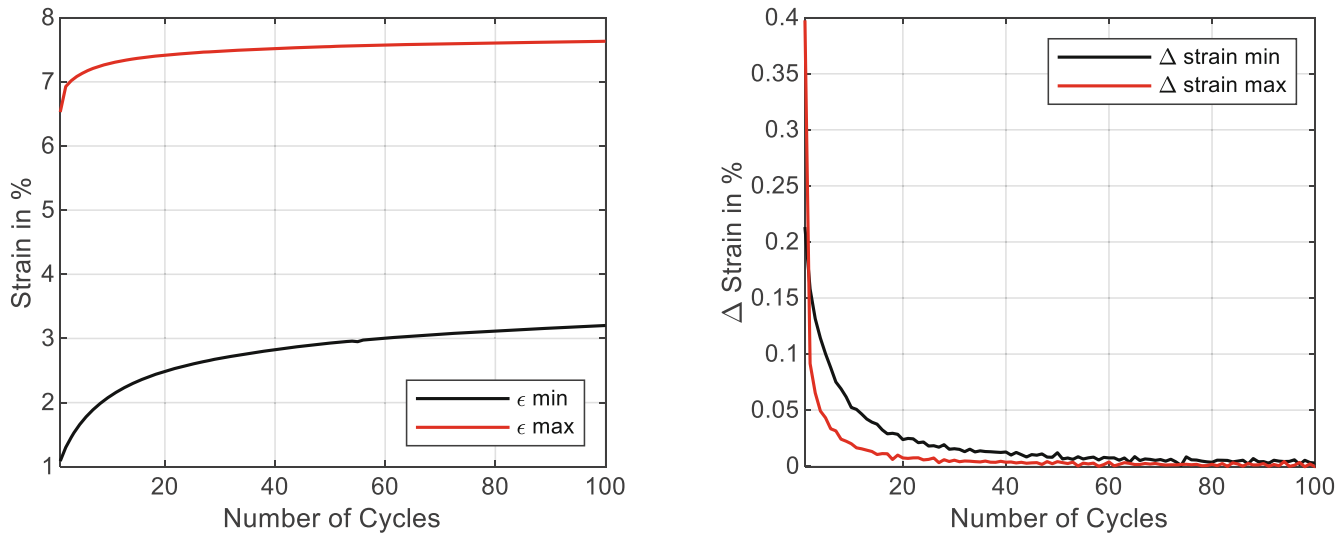

FIGURE 4 Outline of the stabilization of max. and min. strain of the NiTi wire under electro-thermal activation with 400 MPa load. The graph on the left shows the degradation of stroke (plastic shakedown) and the shift of the working point (ratchetting) of the sample. The graph on the right shows the difference in strain between each cycle and the preceding one (derivative) for max. and min. strain.

no stress applied, a certain portion of twinned martensite is formed because of the SMA wire's intrinsic two-way-effect (TWE) as described in.[40] A stable detwinned martensite is only formed after the first activation cycle when cooling under tensile stress. This is also evident in many results in the following subsections.

As criterion for the stability of the sample after the training, the derivative of strain Δ_{strain} is used. The evolution of the derivative for max. and min. strain with the training cycles is depicted in Figure 4 on the right. The chosen threshold value for Δ_{strain} for a functional stability is 0.005%, which is reached for the max. strain after 30 cycles and for the min. strain after 90 cycles. The result after 100 cycles is a $\Delta_{strain\ max}$ of 0.000% and a $\Delta_{strain\ min}$ of 0.003%.

The resistance evolves according to the strain, which is displayed in Figure 3 on the right. Neglecting the inconsistency of the first cycle (green), the martensite resistance starts at 24.4 Ω and rises to 24.7 Ω (red) with the training, due to the increased absolute length of the wire. Because of the reducing contraction, which leads to an increased minimum length, the austenitic resistance starts at 20.5 Ω (green) and ends up at 22.5 Ω (red) after 100 cycles. Before the start of phase transformation and after the transformation is finished, the temperature influence on the wire resistance predominates and the typical increase in resistance occurs, visible in Figure 3 on right and in the resistance signal in Figure 2. It is pronounced at the start of transformation as the martensite slowly heats to A_s temperature. Overheating does not occur, which is why the curvature in the resistance signal is not mirrored in the area of full contraction.

3.2 | Mechanical training

The mechanical training corresponds to cyclic tensile tests with a maximum strain of 5.5%. The wire is heated with controlled electrical power of 0.35 W to reach an initial upper plateau stress (UPS) of about 450 MPa. For low strain rates, leading to isothermal experiments, the wire temperature can be assumed as constant, when the electrical power is constant. In Figure 5, the timing of the first ten training cycles of the with a strain rate of 0.01 s^{-1} is illustrated.

The values of voltage, current and resistance react to the deformation of the wire. The stress signal evolves with progressing cycles, and remanent strain as well as a drop in UPS are recognizable. The change in shape of the stress–strain-hysteresis over 100 tensile cycles is displayed in Figure 6 on the left. The cause, as already explained in Section 3.1 lies in the in microstructural changes within the SMA, which is in thus case induced by repeated loading and unloading in a high temperature state. The level of the UPS drops from about 455 MPa in the 1st cycle to 383 MPa (both at 3% strain) in the last cycle. While that happens the negative slope in the transformation plateau evolves to a constant one. The stress at 5.5% increases from 450 to 468 MPa.

The lower plateau stress (LPS) starts at 190 MPa (at 3%) and, also because auf an increase in slope, rises to 205 MPa. Overall, the hysteresis becomes narrower with the mechanical training. The plastic shakedown manifests in the remanent

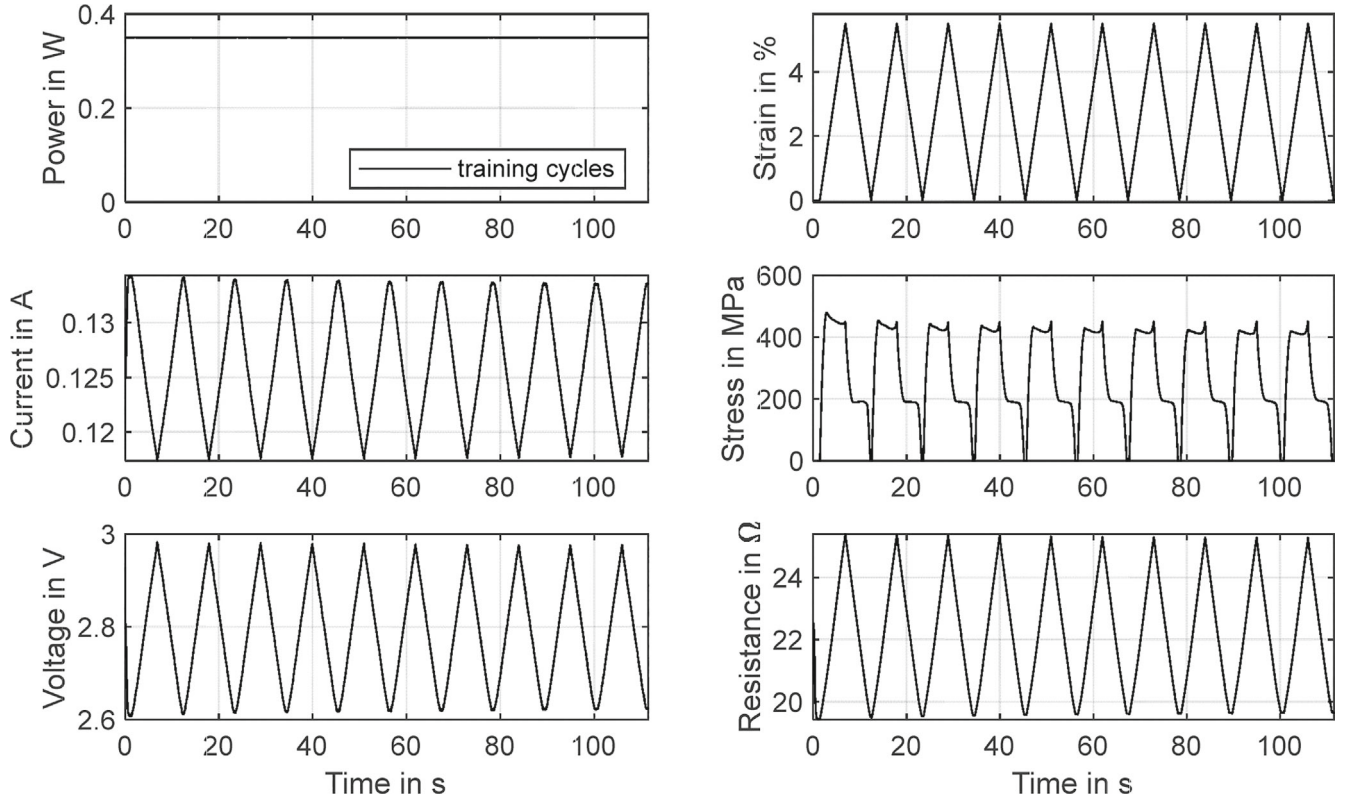

FIGURE 5 Measurement data of the first ten cycles of the mechanical training plotted over time. Presented are the loading and unloading signal with a strain rate of 0.01 s^{-1} at a constant electrical heating power of 0.35 W. Also, the resulting values of current, voltage, resistance and stress are depicted.

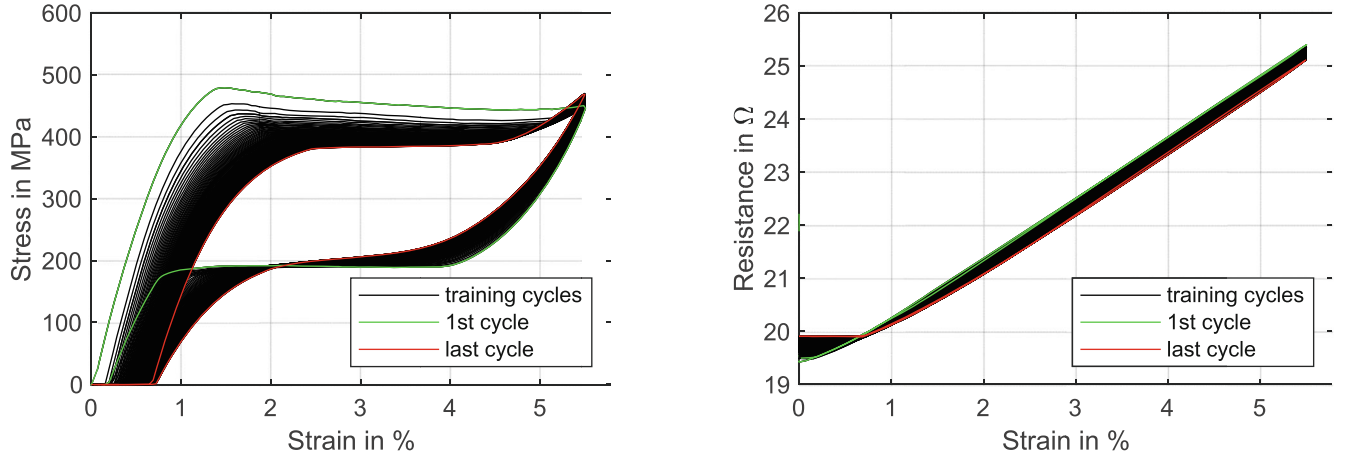

FIGURE 6 Results of the mechanical training with 100 cycles of 5.5% strain and 0.35 W heating power. The left plot illustrates the evolution of stress versus strain and the plot on the right the resistance versus strain behavior. First and last cycle are highlighted in color.

strain ε_{rem} that is represented in Figure 7 on the left, where the max. value of 0.72% is reached after 100 cycles. Equal to the thermal training, a Δ_{strain} of 0.005% is set as threshold of the stability criterion, which is reached after 77 cycles. The evolution of the derivative of remanent strain Δ_{strain} is displayed in Figure 7 on the right.

The resistance signal, represented in Figure 6 on the right, shows an almost linear behavior in relation to strain. In the 1st cycle the resistance starts at 19.5 Ω in full stress-free austenite and increases to 25.4 Ω at the end of the transformation plateau. After 100 tensile cycles to 5.5% strain, this maximum value drops to 25.1 Ω, while the minimum value increases to 19.9 Ω resulting from the remanent strain. In the area of the austenitic branch, the resistance signal shows

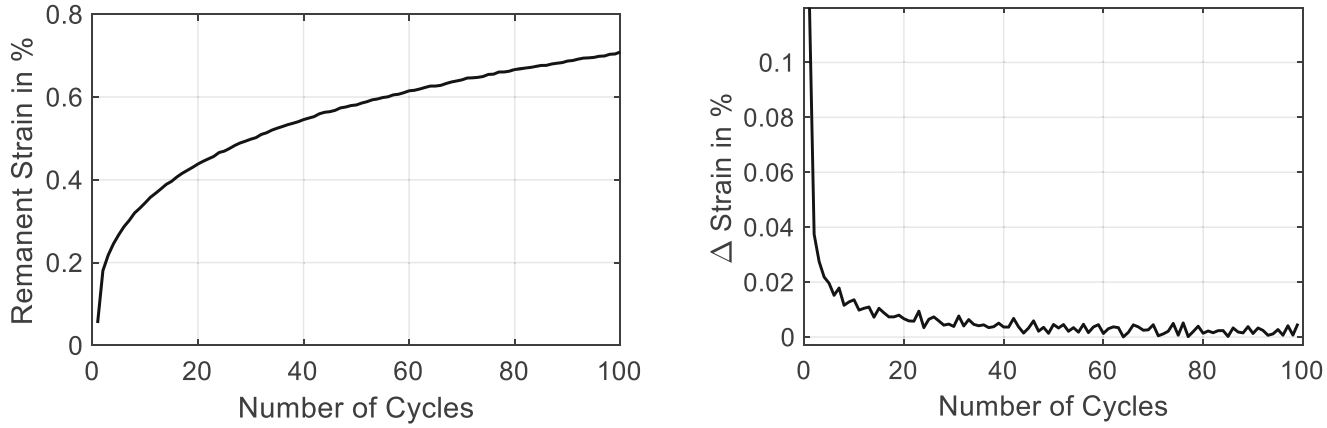

FIGURE 7 The graph on the left outlines the formation of remanent strain over the cycles of the mechanical training with a Joule heated wire sample. The graph on the right illustrates development the derivative of remanent strain over the training cycles.

a lower slope before the UPS is reached. In the linear region, a decrease in resistance between 1st and last cycle of 0.3 Ω is observed.

3.3 | Characterization based on tensile tests

In the following, the execution and results of the first part of the characterization method are discussed. It is called "basic characterization" and consists of a set of several tensile tests with varying heating power and strain. With the experimental data, many material parameters like Young's modulus, width of the mechanical hysteresis and resistivity are determined. The basic characterization is performed with each version of training: the untreated wire as it comes from the manufacturer, the wire with an additional mechanical training as described in Section 3.1 and the wire with an additional thermal training as described in Section 3.2. The results of stress and resistance in relation to strain for each sample are graphically displayed in Figure 8. The maximum strain ε_{max} results of the strain necessary to reach 200 MPa of stress in martensite at room temperature. No offset caused by remanent strain is subtracted, and every experiment starts at the position of L_0 as described in Section 2.

The basic characterization consists of five tensile tests with four different power values. The power levels are identified in preliminary tests of the untreated wire sample and are defined by the UPS of the tensile tests. The highest power is set to produce a UPS of around 550 MPa (+/− 20 MPa), with the UPS of medium and low power lying 100 MPa, respectively 200 MPa lower. Higher stresses result in plastic deformation of the NiTi wire and are not producing significant results from an application perspective because of low fatigue life. The strain rate is set to 0.01 s^{-1} for all tensile experiments. The experiments plotted over time can be found in the "Data S1" section. Two tests are run with only a measurement current of 10 mA applied, which produces a power of around 1 mW. That does not measurably affect the wire temperature. The sequence of the tensile tests for the basic characterization starts with these experiments with no electrical heating, aiming to measure the detwinning of the martensite (black curves in Figure 8) as well as the elastic branch of detwinned martensite (red curves in Figure 8). The power is then gradually increased to 0.29 W (green), 0.35 W (pink) and 0.41 W (blue).

For the untreated wire, a maximum strain of 5.5% is set. The first test with no heating power shows almost no intrinsic TWE, a transformation plateau with a stress starting at 30 MPa and rising to 80 MPa is recognizable. The stress slowly rises between 0.2% and 4%, where the slope increases and leads to 210 MPa at 5.5% strain. The usual explanation for this behavior is the reorientation from twinned martensite (of which the macroscopic geometry with no stress applied corresponds to that of austenite) to detwinned martensite. However, Churchill et al. and Gori et al. showed that "Flexinol", as many other NiTi actuator wires as well, form R-phase fractions when cooling down from austenite at low stresses.[27,28] The R-phase does not have a significant influence on the mechanical properties of NiTi, which is why it is often neglected. Although, when considering the resistance data of the untreated wire in Figure 8, its influence on the sensor characteristics becomes clear. When using a passive SMA actuator wire as a position sensor as can be done for example in an antagonistic wire

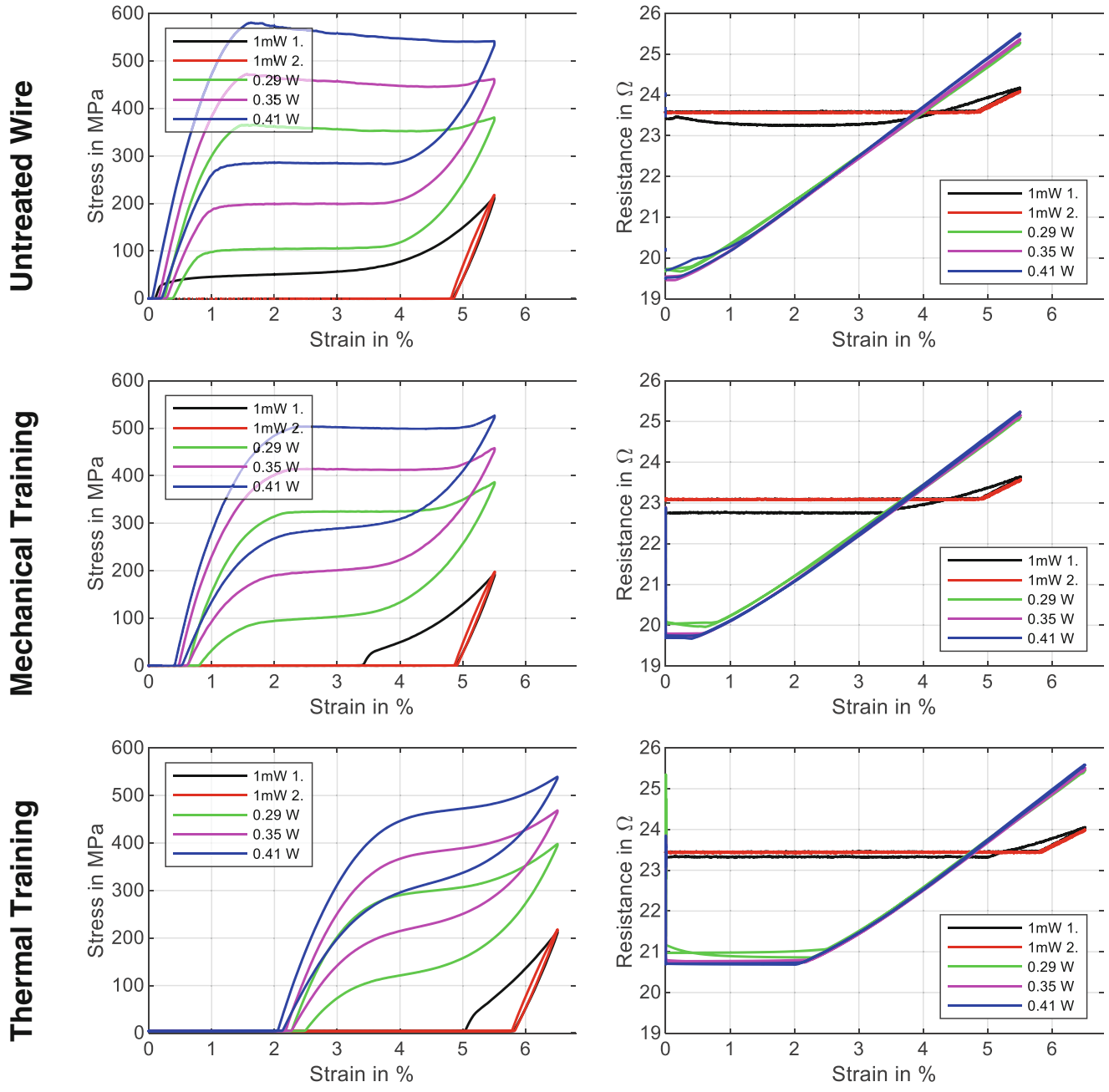

FIGURE 8 Results of the basic characterization tensile tests of three differently trained NiTi wire samples. The left column shows the stress versus strain hysteresis for heating powers from 1 mW to 0.41 W and the right column illustrates the corresponding resistance versus strain plot.

setup, a linear behavior of this wire is expected. In this case however, the hammock shaped resistance-strain curve makes the signal interpretation of a passive wire more difficult.

The initial value of the resistance of the "1 mW 1." test is at a higher level than expected from martensite at L_0. The explanation might be attributed to the heightened resistivity found within the partially present R-phase (ρ_R) of the alloy. After a small increase of the resistance from 23.4 to 23.5 Ω, the resistance signal forms a hammock shape where it drops to 23.2 Ω at 2.2% of strain, and then starts to slowly increase. The maximum value in elastically strained, detwinned martensite at 5.5% strain amounts to 24.2 Ω. The conclusion of these observations is that the crystal lattice of the NiTi wire transforms to a mixture of martensite phase in twinned configuration with a large portion of R-Phase when cooled down

from austenite under stress-free conditions. During the tensile test, the R-phase is detwinned and deformed to martensite phase, which is detwinned at the same time.

The second tensile test with no heating power results in a linear resistance behavior, starting at a constant resistance of 23.6 Ω as long as the wire is slack and reaching 24.1 Ω at the peak. The mechanical behavior of the twinned martensite is elastic, starting at 4.8% with a neglectable hysteresis. The low-, medium- and high-power experiments show properties similar to each other, while the mechanical hysteresis moves to higher levels with increased power, respectively wire temperature. The 0.29 W test results in a hysteresis width of 250 MPa. With increasing power, the hysteresis width increases slightly leading to a width of 258 MPa at 0.35 W and 273 MPa at 0.41 W. The width of the hysteresis, as well as UPS and LPS (displayed in Table 1) are measured at the strain value ε_{hyst} halfway through the loading cycle that calculates with

$$\varepsilon_{hyst} = \frac{\varepsilon_{rem} + \varepsilon_{max}}{2}. \tag{4}$$

The resistance signals of these tensile tests appear to behave linear but feature a curvature change where the austenitic branch ends and at the end of the transformation plateau. The latter is not well pronounced in the experiments displayed here, as the tensile test does not fully enter the elastic branch of the stress induced martensite. The slope of resistance in the elastic branches of austenite and martensite differ from one another, due to their difference in resistivity. Both their slopes are lower than the slope in the region of the transformation plateau, which is to be observed on close inspection in Figure 8. The reason for this behavior can be found in the complex Poisson's ratio ν of NiTi.[41] While the resistivity ρ of an SMA wire at a certain temperature is approximated by

$$\rho = R \times \frac{A}{L}. \tag{5}$$

where R is the measured resistance, L is the current wire length and A the current cross-sectional area of the wire, which is calculated with

$$A = \frac{\pi}{4} \times d_0^2 \times (1 - \nu \times \varepsilon)^2 \tag{6}$$

and thus, depends on the variables strain ε and Poisson's ratio ν. The different resistivities of austenite ρ_A and martensite ρ_M do not explain a steeper slope in the transformation plateau. They are quite similar with martensite having a slightly

TABLE 1 Collection of the material properties extracted from the characterization by tensile experiments for 3 differently trained wire samples.

Value	Untreated wire	Mechanical training	Thermal training
ε_{max} in %	5.5	5.5	6.5
ε_{rem} in %	–	0.39	1.63
TWE in %	0.12	3.42	5.05
σ at ε_{max} in MPa	541	526	537
UPS in MPa	557	502	457
LPS in MPa	284	289	307
Hysteresis width in MPa	273	213	150
Hysteresis area in J	5.0	3.5	2.0
E_A in GPa	75.2	70.7	52.3
E_M in GPa	37.2	36.2	35.5
ρ_A in 10^{-7} Ωm	8.06	7.95	8.08
ρ_M in 10^{-7} Ωm	8.66	8.53	8.50
ρ_R in 10^{-7} Ωm	9.57	–	–
ΔR max. in Ω	6	5.5	4.9

higher value. The alloys resistivity gradually changes with the evolving phase fractions. However, an increased ν in the transformation plateau suits as an explanation, as Equations (5) and (6) demonstrate. For elastic deformation of metallic alloys ν is typically in the region of 0.33, while (quasi-)plastic deformation leads to isochoric behavior and a Poisson's ratio of 0.5. This indicates that the nonlinearity in wire resistance data under tensile loads results from the nonlinear Poisson's ratio of NiTi.[41] The behavior can also be observed in the experimental results of Lewis et al.[14] However, the assumption needs further investigation.

Also, it is to be observed in the measurement data that the mean slope of the resistance versus strain plot increases with increasing power, leading to a maximum resistance value of 25.5 Ω. In Figure 9 additional tensile tests for the evaluation of remanent strain ε_{rem}, Young's modulus of martensite phase (E_M) and austenite phase (E_A) as well as the estimation of actuation stroke are displayed. The tensile tests in the elastic region of full austenite and fully detwinned martensite are performed up to a stress of about 400 MPa. The untreated sample (Figure 9A) does not exhibit any remanent strain, as it is not cycled before the basic characterization. The quasi-plastic residual strain in martensitic phase detwinned with 400 MPa and 6.5% strain is 5.3%. The elastic moduli are displayed together with all other material properties in Table 1. They are calculated by a linear approximation of the slope of the elastic branches.

Examining the basic characterization of the mechanical training, an increase in intrinsic TWE to 3.5% can be found in Figure 8 in the middle row. With that the appearance of the R-phase also seems to be reduced, as the resistance is lower than in the previous experiment although the wire length is increased to 103.5 mm. The resistance levels in general are slightly lower compared to the untreated wire, except for the initial values with heating power, matching the results of the mechanical training. The results of mechanical hysteresis are also comparable to the results in Section 3.2, where the UPS decreases, and the slopes of the plateaus increase. The active strain, where the wire is actually loaded, in the basic characterization is reduced to a maximum of 5%. The residual strain extracted from the full austenite data in Figure 9B is 0.37%.

Moving to the results of the thermal training, it can be determined in Section 3.1 that the ratcheting and plastic shakedown move and reduce the working range of the SMA actuator wire. Therefore, the maximum strain of the basic characterization must be increased to 6.5%. The maximum active strain, where the wire is not slack, is reduced to 4.45% starting at 2.05% with a power of 0.41 W. The intrinsic TWE extracted from the first cold state experiment is 5.05%. The remanent strain is 1.6%, as visible in Figure 9C. The shape of the hysteresis is changed dramatically compared to the untreated wire, which is also reflected in the hysteresis area listed in Table 1. It is compressed in strain direction, the transformation plateaus are less pronounced and a more homogeneous transition from the austenite branch, through the transformation plateau to the stress induced martensite branch is observed. The hysteresis width is reduced to about 150 MPa.

There is no more evidence of the R-phase in the resistance results of cold state tensile tests. The initial resistance level is unchanged compared to the untreated wire, although the wire length is increased as a result of the training. The course of the resistance signal of the austenitic tests is shifted in the direction of positive strain and reaches a maximum value of 25.6 Ω. That corresponds almost to the maximum of the untreated wire with 1% lower strain. The reason can be found in the higher starting strain of the mechanical response and the increased nonlinearity of the resistance curve. This results from the changed transformation behavior, which also manifests in the mechanical hysteresis. When studying Figure 9

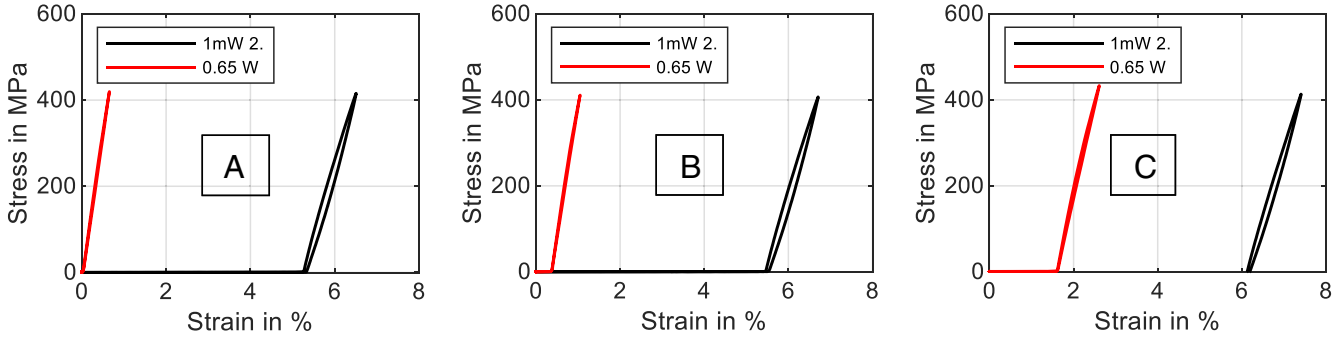

FIGURE 9 Results of tensile tests with maximum power (0.65 W) resulting in full austenite (red) and without heating power (1 mW) resulting in full detwinned martensite (black), while the stress is restricted to 400 MPa. The data for the three differently treated samples are depicted. "A": untrained wire, "B" mechanically trained wire, "C" thermally trained wire.

and comparing the slopes of the elastic martensite and austenite branches, it is apparent that both training methods reduce the E_A, of which the exact values are displayed in Table 1.

To sum up, the results of the characterization with tensile tests leads to the conclusion, that training the wire with either of the proposed methods influences the sensor and actuator characteristics of an SMA wire. The stability of the R-phase is reduced with both training methods. This leads to easier signal interpretation on thermally passive wires, that are stretched to use as position sensors. The working point of the actuator shifts, especially after thermal cycling and the stroke is also reduced.

To design an SMA actuator system, the tensile tests up to 400 MPa in full austenite and fully detwinned martensite (Figure 9) are a proper tool to graphically estimate the maximum stroke that an SMA actuator generates in combination with a certain bias load. By drawing the characteristics of the bias system (e.g., a linear spring) in the stress–strain diagram, the stroke can easily be read from the intersection points with austenite and martensite curve. With the help of the resistance data, the necessary voltage and current supply can already be determined in an exact manner. The resistance range for self-sensing is also already known, which helps for the preliminary design of the electronics. For the exact behavior of the sensor signal however, the results of actuator tests, as discussed in the following paragraph, are necessary.

3.4 | Characterization of the actuator behavior

In this subsection, the results of actuation experiments with the introduced wire samples are discussed. The goal is to determine the influence of the different training methods on the actuator and sensor properties of the NiTi wire. These properties are the functional stability under high loads, the output stroke and the characteristics of the resistance signal. The characterization is performed with four different loads. In the low stress region, a spring load corresponding a pre-stress of 100 MPa and a max. stress of 200 MPa and a constant load corresponding a stress of 200 MPa are examined. In the high stress region, a spring load generating 200 to 400 MPa of stress as well as a constant load with 400 MPa are investigated. The experimental data plotted over time is displayed for one experiment in the main text. The remaining experimental data over time can be found in the "Data S1" section. The section is structured after the load used in the experiment, so that the characteristics of the samples can be compared to each other by means of the same load. For the evaluation of the actuation tests and the samples functional stability under a certain load, the activation cycle is repeated three times for each experiment. The first cycle usually defers from the remaining cycles due to the wires "load history". In the following this is to be observed for constant load experiments only. Due to the experimental procedure, a preliminary actuation test is necessary for the spring force experiments to set the right pre-stress.

3.4.1 | Low stress actuation with spring load

For all following experiments a triangular signal with controlled current is used to heat the SMA wire and trigger the transformation. The amplitude of the electrical current is defined in preliminary tests to ensure a fully transformed austenite state for each stress level. For the experiments with low stress, the peak current is set to 160 mA. As displayed in Figure 10 the cycle time of the signal is 40 s to ensure a clean force control of the linear drive in the test rig and enough time for the wire to cool down at low currents. The current signal has an offset of 10 mA for a continuous resistance measurement. The pre-stressing and unloading path, visible in stress versus time in Figure 10, are not depicted in the strain and power plots discussed in the following, as they are not part of the actual experiment. The timing plots of all remaining experiments can be found in the "Data S1" section.

It is expected that the results of the low stress experiments show a good functional stability, and that no difference is to be observed between the first and third cycle. The stability is measured in the same manner as described in Section 3.1. In fact, these expectations are met by all three samples as is illustrated in Figure 11, where the three cycles cannot be distinguished in each case. No buildup of residual strain or shift in working point is observed. For one sample, the heating and cooling are indicated with arrows in the plot in Figure 11. This can be transferred to the rest of the data in this work, as the pattern stays the same.

The stroke of the untreated sample is 4.8% and is reduced by the plastic shakedown and ratcheting in both results of the trainings. The mechanically trained wire has an actuator stroke of 4.4% and the thermal training reduces the stroke to 4%. Here it is to be noted that the working range is moved by about 1% compared to the mechanical training, as was already observable in the basic characterization. Instead of strain versus temperature plots, in Joule heated experiments strain

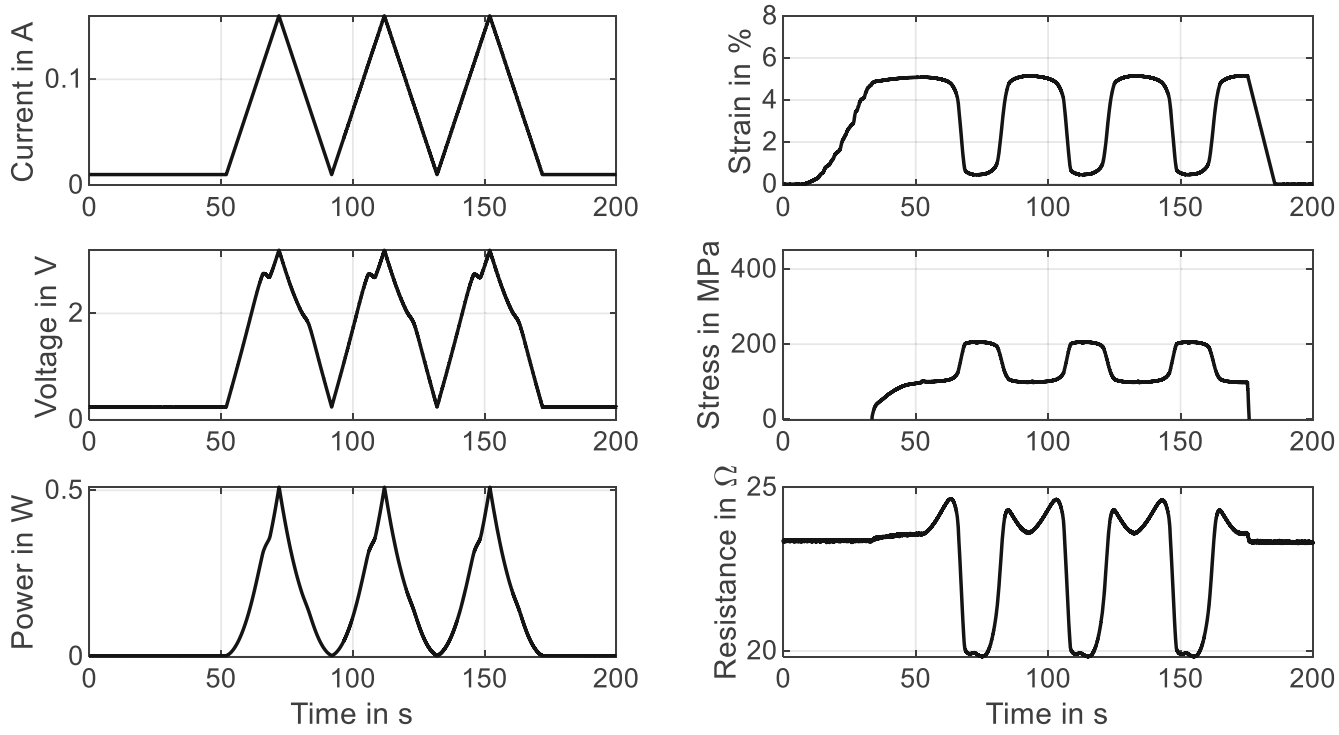

FIGURE 10 Timing of all measurements of the actuator experiment with controlled current in triangular shape, using the untreated wire sample. The bias is a linear spring load corresponding 100 MPa of prestress and 200 MPa maximum load.

versus electrical power plots are investigated. Without further ado, the electrical heating power cannot be correlated to a certain temperature. But due to the slow cycling the behavior is qualitatively very similar to strain versus temperature. In general, it is also possible to extract transformation powers as a replacement for the transformation temperatures. But as they strongly depend on the ambient temperature, this is neglected in this work.

It can be observed in the strain-power hysteresis in Figure 11, is an analogy to the results of the mechanical hysteresis. The training reduces the hysteresis width and changes the slopes. The transformation points are less pronounced and especially the thermal training results in a homogeneous transition from martensite to austenite. While the untreated wire forms a curve parallel to the x-axis when in full austenite, the trained wires still have a downward slope. A higher power would lead to slightly increasing contraction.

Looking at the resistance over strain behavior in the left column of Figure 11, a distinct hysteresis is recognized. The resistance of the untreated wire starts at 23.5 Ω in cold state and drops to 19.9 Ω in full austenite. This corresponds to a change in resistance of 15%. The peak in resistance in the heating path results from the temperature influence before the main part of the phase transformation starts. After that, the heating path follows the strain in a linear manner until the minimum strain is reached and an increase in electrical power leads to another temperature related rise of the resistance. The course of the cooling is nonlinear and two changes in slope at about 1% and 4% of strain are recognizable. This hysteretic behavior in resistance is another evidence of the R-phase that forms when the NiTi wire cools down from austenite at low stresses. The influence of this intermediate phase on the resistance versus power plot can be observed in the first row and second column of Figure 11. The heating branch of strain and resistance both show distinct and overlapping characteristics in the area of the phase transformation. The cooling branch is different, and the resistance shows a round and homogenous shape, not directly following the strain of the wire.

The results of the mechanical training show a reduced width of the resistance hysteresis related to strain and power. This means that the formation of R-phase is reduced, as can also be observed in Section 3.3. The thermal training reduces it even further, and the hysteresis is reduced to a max. width of 0.3 Ω, coming from 1 Ω for the untreated wire. Also, the course of the cooling branch of the resistance and strain versus power move closer together.

At this point, the conclusion for low stress actuation is, that a training reduces the maximum stroke that can be reached with the actuator and a thermal training also moves the working point due to the plastic deformation. This confirms the findings of the tensile tests. On the other hand, the decrease of the resistance-strain hysteresis is remarkable, especially

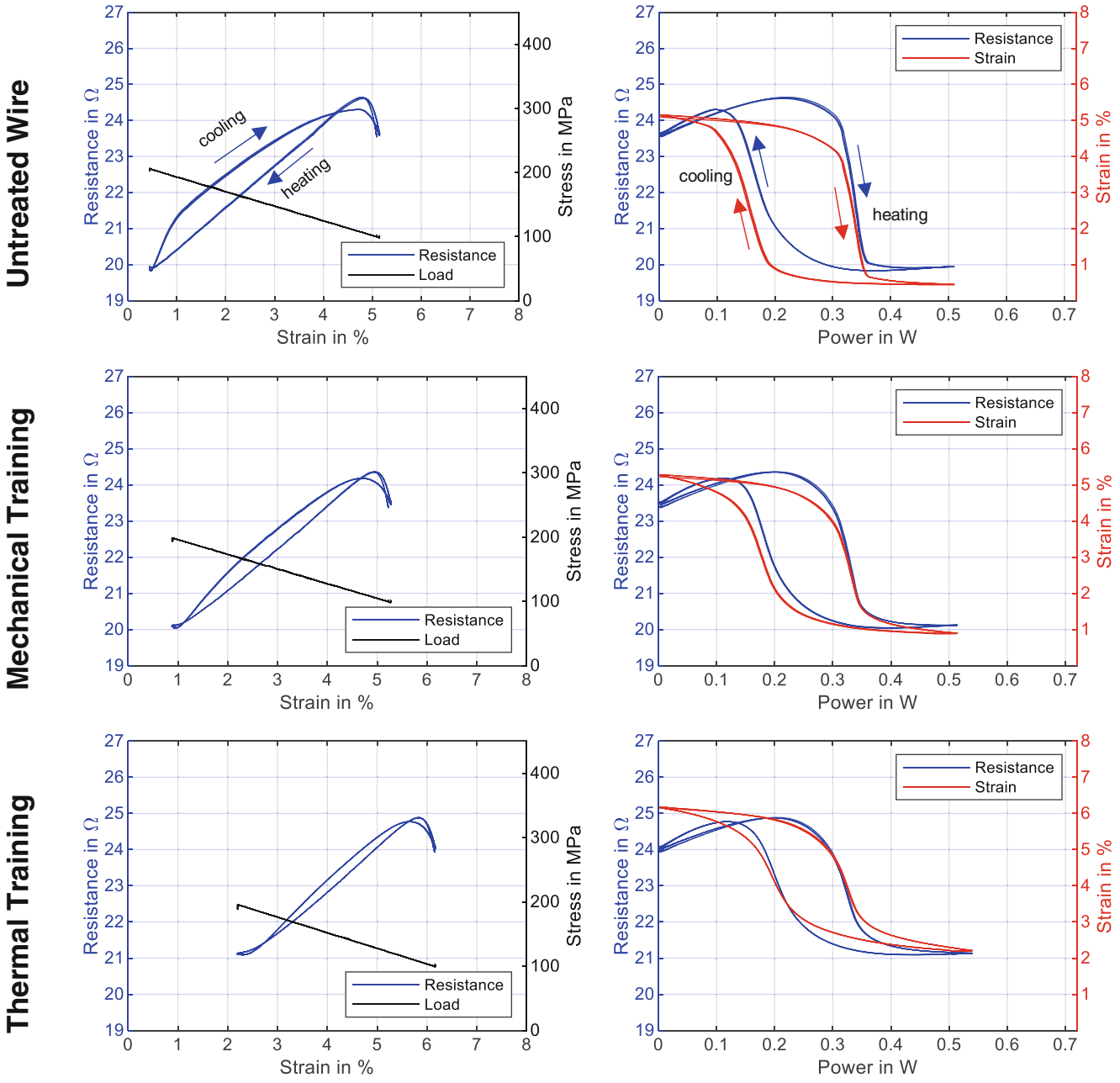

FIGURE 11 Actuator experiments with a linear spring load corresponding 100 MPa of pre-stress and 200 MPa of maximum load. Results for the three differently trained samples are depicted. The left column displays resistance and stress versus strain and the right column resistance and strain versus power.

due to the thermal training. It has a positive effect on the self-sensing capability, as complicated control algorithms to compensate the hysteresis are not necessary.

3.4.2 | Low stress actuation with constant load

The test parameters in this section are unchanged to Section 3.4.1, except for the load that is now kept constant at 200 MPa. The first cycle of each constant load experiments starts at a lower martensitic strain than the following cycles. This is because a tensile load of 200 MPa without thermal cycling does not fully re-orient the martensite crystal lattice and a small

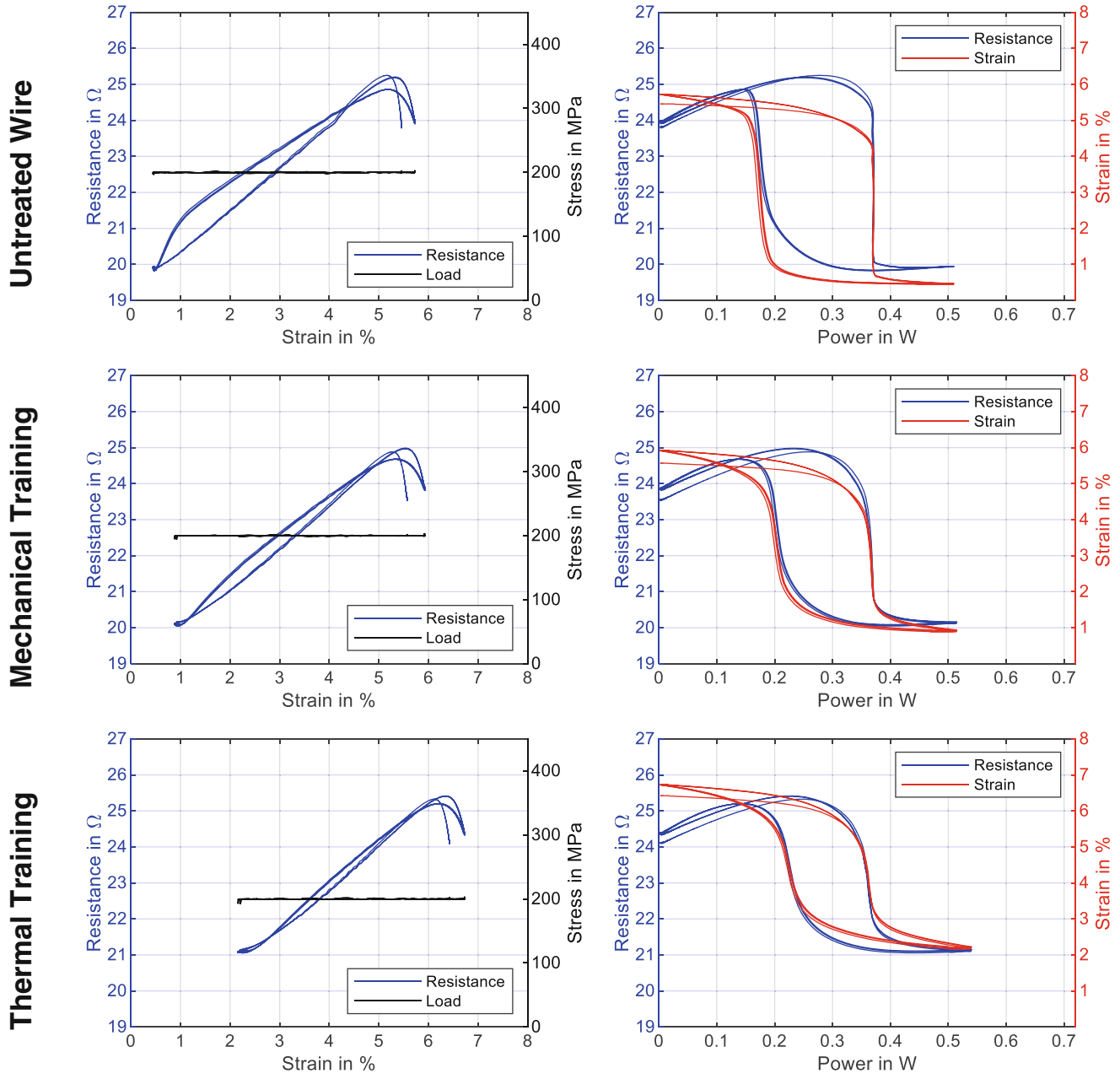

FIGURE 12 Actuator experiments with a constant load of 200 MPa. Results for the three differently trained samples are depicted. The left column displays resistance and stress versus strain and the right column resistance and strain versus power.

amount of twinned martensite is left. After the first heating cycle and cooling under stress, the crystal lattice transforms to a higher amount of detwinned martensite, and results in an increased strain.

This phenomenon has to be taken into account, when SMA driven systems are designed. Especially the mounting procedure of the SMA wires and commissioning of the final system is affected. None of the samples show stability issues. With the higher stress in martensite, the maximum strain of the SMA wire is increased and with that also the stroke of the actuator. As depicted in Figure 12, the stroke of the untreated wire amounts to 5.3%. The mechanical training reduces it to 5% and the thermally trained wire produces a stroke of 4.6%. This means that the stroke is increased by roughly 0.5% for all training variants due to the higher bias stress.

The slope of the strain versus power plot of the untreated wire is almost vertical when the phase transformation happens. Compared to a spring load, the stress-dependent transformation temperature stays the same and is not

depending on the strain. A spring load on the other hand, leads to a changing transformation temperature, increasing with decreasing strain. The shapes of the strain-power hysteresis change in the same manner as before. Their width decreases, transformation points evolve to transformation areas and the austenitic branch keeps a slight downward slope.

The general characteristics of the wire resistance relates to that of Section 3.4.1. The R-phase related resistance-strain hysteresis is recognizable in a similar way. However, the second curvature change at higher strains, that is observed with the spring load, is gone. This leads to a smaller hysteresis area, with a maximum width of 1 Ω for the untreated wire. As before, both trainings reduce the hysteresis width and area. The thermally trained wire shows a max. hysteresis width of only 0.1 Ω. The round shape of the cooling branch in the resistance-power plot, that does not follow the course of the strain is most pronounced in the results of the untreated wire in the first row and second column in Figure 12. Both trainings reduce this phenomenon. The training creates a less distinct transformation and a reduced R-phase proportion, the shape of the resistance-power hysteresis becomes smoother and moves closer to the strain-power plot.

3.4.3 | High stress actuation with spring load

As the goal of the training procedure is to reach a stable behavior of the SMA wire also under high stress, the following results show the necessity for this measure and the outcome for the two methods that are compared. For the high stress actuation experiments, the maximum heating current is increased to 180 mA, while the cycle time is unchanged at 40 s. The pre-stress of the linear spring corresponds to a stress of 200 MPa and the maximum stress is 400 MPa. The average stroke of the untreated SMA wire is 4.9% but reduces about 0.05% with each cycle. That is ten times higher than the stability criterion defined in Section 3.1.

As expected, the untreated wire, as conditioned by the manufacturer, is not stable at this stress level. The mechanical training improves the stability to 0.02% strain difference between the cycles at an average stroke of 4.6%, while the thermal training shows a stable behavior with 4.1% of stroke.

As displayed in the left column of Figure 13, the hysteresis of resistance in relation to strain is reduced drastically with the higher stress in all three samples. What stays recognizable are the loops at the beginning of the activation and at the end of the transformation. They are a result of the thermal hysteresis and the difference between martensite and austenite transformation temperatures. Neglecting these loops, the main course of the resistance signal behaves linear with almost no hysteresis. An exception is made by the untreated wire sample, where a slight hysteresis due to an increase in resistance is observed starting at 4.5% of strain and 250 MPa. The increased material stress suppresses the formation of the R-phase, while both trainings additionally reduce the effect. A stable behavior of the SMA wire with the examined spring tension is only achieved by prior thermal training. The mechanical cycling does unfortunately not create a sufficiently stable actuator. Having future production lines in mind, where actuator need to be trained for their specific application, the mechanical training would have been beneficial due to faster and easier implementation. It should be examined in further research, if a prior thermal training with the exact load as used in the actuator application (in this case 200–400 MPa spring load), would lead to the same stable behavior and better stroke output. Then, also the influence of the applied training load on the reduction of the R-phase is of interest.

Looking at the data in the power domain on the right column of Figure 13, the linear spring force leads to a similarly angled behavior in the transformation region like in Section 3.4.1. As before, training increases this angle, and the transformation start is less pronounced. A higher stress increases the quality of the resistance signal for self-sensing by eliminating the hysteresis almost to full extend. This makes the data easier to interpret but comes with the cost of reduced stroke and a training procedure for a stable behavior is required.

3.4.4 | High stress actuation with constant load

The final experiments discussed in this article are the actuation tests with 400 MPa of constant load. As before, the wire is Joule heated by a current controlled triangular signal with 180 mA of amplitude and 40 s cycle time. The results for all

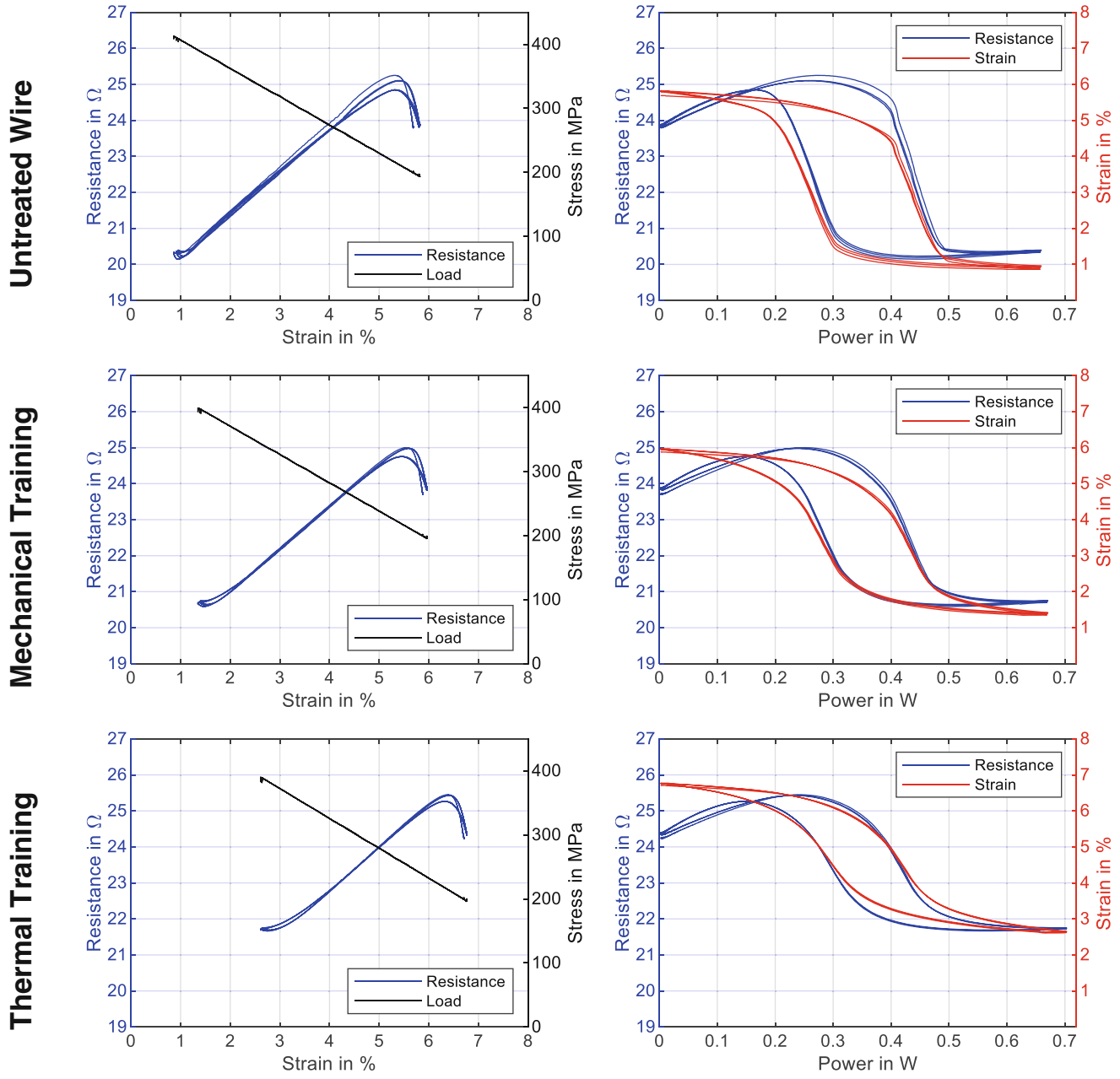

FIGURE 13 Actuator experiments with a linear spring load corresponding 200 MPa of pre-stress and 400 MPa of maximum load. Results for the three differently trained samples are depicted. The left column displays resistance and stress versus strain and the right column resistance and strain versus power diagrams.

samples are displayed in Figure 14 in the strain and power domain. It can be deduced from the previous sections that the untreated wire sample is not stable and basically the first three cycles of the training method displayed in Section 3.1 are to be observed here as well.

Pre-stressing the untreated SMA wire in twinned martensite to 400 MPa results in a strain of 6.6%. After the first activation cycle the martensitic strain increases to roughly 7% and an average stroke of 5.7% for the untreated wire is there. The trained variants behave similarly with 5.4% of stroke resulting from the mechanical training and 4.8% from the thermal training.

The mechanical training does not create a functional stability at 400 MPa actuation stress, as can be expected from the experiments discussed in previous sections. The thermally trained wire can on the other hand be expected to behave

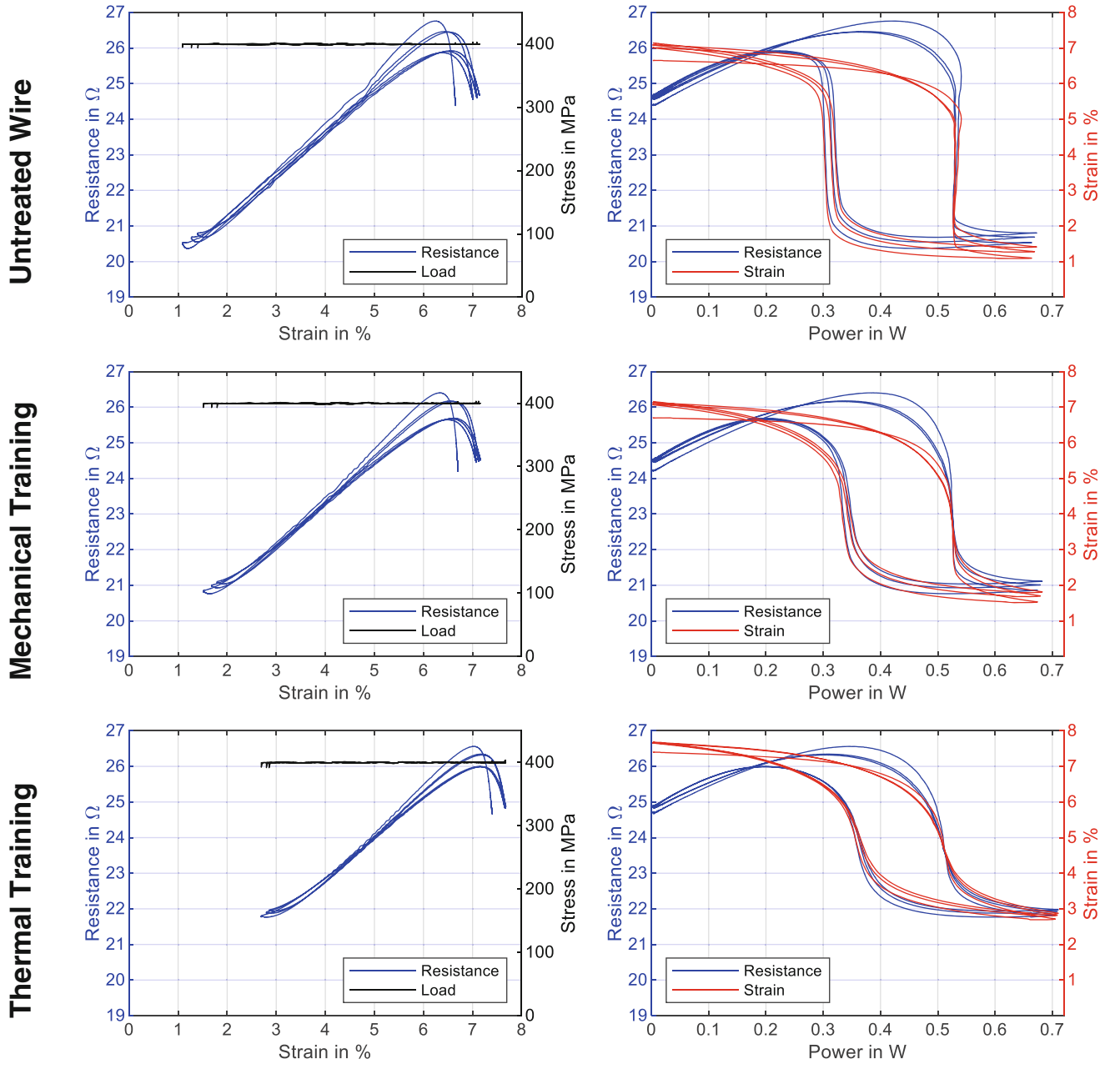

FIGURE 14 Actuator experiments with a constant load of 400 MPa. Results for the three differently trained samples are depicted. The left column displays resistance and stress versus strain and the right column resistance and strain versus power.

stable. The experiments discussed here have equal parameters like the thermal training, which met the stability criterion after 100 cycles. Therefore, only the first cycle of the actuation test of the thermally trained SMA wire shows the typical gap, known from the other experiments discussed in the previous sections.

In the first cycles of all three samples the resistance peak at the start of activation is higher than the following two. An explanation can be, that fractions of the R-phase with higher resistivity are present. It is apparent that for all three wire samples, the resistance versus strain behavior is still less hysteretic than these of the low stress experiments. However, the loops at the start and end of the heating phase are more pronounced than with 200–400 MPa of stress in Section 3.4.3.

The shape and behavior of the resistance and strain hysteresis in the power domain are similar to those in Section 3.4.2, with almost vertical course in the transformation for the untreated sample and the same evolution with the training as

described previously. Different than in the low stress results, the resistance follows the strain in a close manner, which leads to the small hysteresis in the strain domain.

It can be derived, that increasing the material stress reduced the resistance hysteresis only so far. The experiments with a constant load of 400 MPa show again slightly larger hysteresis for resistance strain, that are not due to the R-phase. The load profile plays a large role in designing SMA-actuator sensor systems and the maximum load is no sufficient information.

4 | CONCLUSION AND OUTLOOK

The article presents a new application-oriented method to characterize SMA wires for their use as Joule heated actuators with self-sensing. By means of the proposed procedures the exact behaviors of resistance and strain for arbitrary loads and different heating powers are investigated. With the help of a custom designed test-rig, all tests are run on the same sample and tensile tests can be compared to actuation tests. Prior to that, various trainings can be performed on the wire sample. The method is not restricted to the parameters used in this work and it is possible to examine any kind of thermal SMA actuator wire from 20 to 100 µm diameter with respect to their suitability for a certain application. Additionally, the tensile tests give us the basic material parameters to compare alloys and trainings.

In this work, the influence of mechanical and thermal training on the material and actuator-sensor properties on the example of "Dynalloy Flexinol HT" are investigated. It can be concluded that the training of an SMA wire should be adapted to the load in the target application. That means that thermal training is to be preferred for an optimal utilization of the stroke. The thermal training reduces the hysteresis in the resistance signal and enables a stable material behavior at loads up to the training stress. Higher bias stresses in an application suppress the R-phase and lead to a more linear resistance curve, which makes the interpretation of the sensor signal easier. With higher stress, a more efficient use of space is enabled. When the actuator force is scaled by wire bundling or transmission stages instead, the installation space does increase. In recent research on soft and bending SMA actuators the findings of this work is able to help improving the actuation performance of the wire, by supporting the choice of the right training.[42–44] Also, the findings of the proposed research can be transferred to these kinds of actuators to improve the understanding and utilization the self-sensing capabilities better.[45]

The proposed methods are to be used in future work to further investigate how to tune certain properties of SMA wires by using specific training parameters. Examining the training with additional waveforms such as square waves, longer cooling periods and also different load profiles will be an essential part of it. Further research on the resistivity and its dependency on the Poisson's ration is also of interest. Therefor a precise and continuous measurement of the wire diameter during the phase transformation is necessary. In general, a manifold of other studies on various parameters and stimuli can be done. Due to its the multifunctionality, the utilized test platform will be at the core of several research topics to come.

In "Part 2" of this work the limits for SMA actuators in high ambient temperatures and how to push them with training and increased material stress are investigated. An exemplary actuator is designed and tested by means of the hardware-in-the-loop feature of the test rig under high ambient temperatures.

AUTHOR CONTRIBUTIONS

Dominik Scholtes: Conceptualization; data curation; formal analysis; investigation; methodology; project administration; resources; software; validation; visualization; writing – original draft; writing – review and editing. **Stefan Seelecke:** Formal analysis; funding acquisition; investigation; methodology; project administration; supervision; writing – original draft; writing – review and editing. **Paul Motzki:** Formal analysis; funding acquisition; methodology; project administration; resources; supervision; writing – original draft; writing – review and editing.

ACKNOWLEDGMENT

Open Access funding enabled and organized by Projekt DEAL.

CONFLICT OF INTEREST STATEMENT

The authors declare no conflict of interest.

PEER REVIEW

The peer review history for this article is available at https://www.webofscience.com/api/gateway/wos/peer-review/10.1002/eng2.12867.

DATA AVAILABILITY STATEMENT

The data that support the findings of this study are available from the corresponding author upon reasonable request.

ORCID

Dominik Scholtes https://orcid.org/0009-0008-5515-4636

REFERENCES

1. Degeratu S, Rotaru P, Manolea G, Manolea HO, Rotaru A. Thermal characteristics of Ni–Ti SMA (shape memory alloy) actuators. *J Therm Anal Calorim*. 2009;97(2):695-700. doi:10.1007/S10973-009-0215-0
2. Fumagalli L, Butera F, Coda A. SmartFlex® NiTi wires for shape memory actuators. *J Mater Eng Perform*. 2009;18(5–6):691-695. doi:10.1007/s11665-009-9407-9
3. Lagoudas DC. *Shape Memory Alloys*. Vol 1. Springer US; 2008. doi:10.1007/978-0-387-47685-8
4. Miller DA, Lagoudas DC. Thermomechanical characterization of NiTiCu and NiTi SMA actuators: influence of plastic strains. *Smart Mater Struct*. 2000;9(5):640-652. doi:10.1088/0964-1726/9/5/308
5. Buehler WJ, Wang FE. A summary of recent research on the nitinol alloys and their potential application in ocean engineering. *Ocean Eng*. 1968;1(1):105-120. doi:10.1016/0029-8018(68)90019-X
6. Crews JH, Buckner GD. Design optimization of a shape memory alloy–actuated robotic catheter. *J Intell Mater Syst Struct*. 2012;23(5):545-562. doi:10.1177/1045389X12436738
7. Antonucci V, Faiella G, Giordano M, Mennella F, Nicolais L. Electrical resistivity study and characterization during NiTi phase transformations. *Thermochim Acta*. 2007;462(1–2):64-69. doi:10.1016/j.tca.2007.05.024
8. Furst SJ, Seelecke S. Modeling and experimental characterization of the stress, strain, and resistance of shape memory alloy actuator wires with controlled power input. *J Intell Mater Syst Struct*. 2012;23(11):1233-1247. doi:10.1177/1045389X12445036
9. Buehler WJ, Gilfrich JV, Wiley RC. Effect of low-temperature phase changes on the mechanical properties of alloys near composition TiNi. *J Appl Phys*. 1962;1475:2-5. doi:10.1063/1.1729603
10. Janocha H, Bonertz T, Pappert G. *Unkonventionelle Aktoren: eine Einführung*. Oldenbourg Wissenschaftsverlag; 2013.
11. Wang T, Ma Z, Rao X, et al. Temperature-dependence of superelastic stress in nanocrystalline NiTi with complete transformation capability. *Intermetallics*. 2020;127:106970. doi:10.1016/J.INTERMET.2020.106970
12. Ling HC, Kaplow R. Stress-induced shape changes and shape memory in the R and Martensite transformations in Equiatomic NiTi. *Metall Trans A, Phys Metall Mater Sci*. 1981;12(12):2101-2111. doi:10.1007/BF02644180
13. Duerig TW, Bhattacharya K. The influence of the R-phase on the Superelastic behavior of NiTi. *Shape Mem Superelasticity*. 2015;1(2):153-161. doi:10.1007/s40830-015-0013-4
14. Lewis N, York A, Seelecke S. Experimental characterization of self-sensing SMA actuators under controlled convective cooling. *Smart Mater Struct*. 2013;22(9):094012. doi:10.1088/0964-1726/22/9/094012
15. Park CH, Son YS. SMA spring-based artificial muscle actuated by hot and cool water using faucet-like valve. 2017;10164:165-174. doi:10.1117/12.2257467
16. Actuator Solutions GmbH. Actuator Solutions GmbH. https://www.actuatorsolutions.de/english/products/ (accessed May 12, 2023)
17. Scholtes D, Seelecke S, Rizzello G, Motzki P. Design of a Compliant Industrial Gripper Driven by a Bistable shape memory alloy actuator. *Proceedings of the ASME Conference on Smart Materials, Adaptive Structures and Intelligent Systems*. 2020. doi:10.1115/SMASIS2020-2204
18. Kazi A, Honold M, Rimkus W, Lokner T, Bäuml M, Köpfer M. SMA actuator for optical image stabilization. ACTUATOR 2018 - 16th International Conference and Exhibition on New Actuators and Drive Systems, Bremen: VDE. 2018 375–378.
19. Uleru GI, Hulea M, Burlacu A. Bio-inspired control system for fingers actuated by multiple SMA actuators. *Biomimetics*. 2022;7(2):62. doi:10.3390/BIOMIMETICS7020062
20. Mandolino MA, Goergen Y, Motzki P, Rizzello G. Design and characterization of a fully integrated continuum robot actuated by shape memory alloy wires, in 2022 IEEE 17th International Conference on Advanced Motion Control, Institute of Electrical and Electronics Engineers (IEEE). 2022, pp. 6–11. doi:10.1109/AMC51637.2022.9729267
21. Cheng C, Cheng J, Huang W. Design and development of a novel SMA actuated multi-DOF soft robot. *IEEE Access*. 2019;7:75073-75080. doi:10.1109/ACCESS.2019.2920632
22. Bevilacqua D, Soleti G, Naso D, Rizzello G, Motzki P. Bio-inspired flapping wing antagonist actuation with SMA wires. *ACTUATOR 2022; International Conference and Exhibition on New Actuator Systems and Applications*. VDE; 2022:81-84.
23. Takimoto A. Relationship between volume fraction of strain-induced Martensite under tension and electrical resistivity in a Ti-Ni SMA wire. *J Phys IV*. 1995;05(C8):C8-C599. doi:10.1051/JP4/199558599
24. Churchill CB, Shaw JA, Iadicola MA. Tips and tricks for characterizing shape memory alloy wire: part 1 – Differential Scanning Calorimetry & Basic Phenomena. *Exp Tech*. 2009;33(1):51-62. doi:10.1111/J.1747-1567.2008.00460.X

25. Shaw JA, Churchill CB, Iadicola MA. Tips and tricks for characterizing shape memory alloy wire: part 2—fundamental isothermal responses. *Exp Tech*. 2008;32(5):55-62. doi:10.1111/J.1747-1567.2008.00410.X
26. Churchill CB, Shaw JA, Iadicola MA. Tips and tricks for characterizing shape memory alloy wire: part 4 - Thermo-mechanical coupling: experimental characterization of active materials series. *Exp Tech*. 2010;34(2):63-80. doi:10.1111/j.1747-1567.2010.00619.x
27. Gori F, Carnevale D, Doro Altan A, Nicosia S, Pennestrì E. A new hysteretic behavior in the electrical resistivity of flexinol shape memory alloys versus temperature. *Int J Thermophys*. 2006;27(3):866-879. doi:10.1007/s10765-006-0060-3
28. Churchill CB, Shaw JA. Shakedown response of conditioned shape memory alloy wire. *Behav Mech Multifunct Compos Mater*. 2008;6929:69291F. doi:10.1117/12.778726
29. Churchill CB, Shaw JA. Thermo-electro-mechanical shakedown response of conditioned shape memory alloy wires. *Proc ASME Conf Smart Mater Adapt Struct Intell Syst, SMASIS2009*. 2009;1:137-148. doi:10.1115/SMASIS2009-1306
30. Furst SJ, Crews JH, Seelecke S. Stress, strain, and resistance behavior of two opposing shape memory alloy actuator wires for resistance-based self-sensing applications. *J Intell Mater Syst Struct*. 2013;24(16):1951-1968. doi:10.1177/1045389X13486715
31. Britz R, Motzki P. Analysis and evaluation of bundled SMA actuator wires. *Sensors Actuators A Phys*. 2021;1-2:113233. doi:10.1016/J.SNA.2021.113233
32. Song SH, Lee JY, Rodrigue H, Choi IS, Kang YJ, Ahn SH. 35 Hz shape memory alloy actuator with bending-twisting mode. *Sci Rep*. 2016;6(February):1-13. doi:10.1038/srep21118
33. Camebridge Mechatronics - Actuators. https://www.cambridgemechatronics.com/en/cml-technology/actuators/ (accessed Aug. 21, 2023)
34. Kirsch SM, Welsch F, Bevilacqua D, et al. SMA antagonistic-micro-wire bundle: first measurement results, SMASIS 2020 - Conference on Smart Materials, Adaptive Structures and Intelligent Systems. 2020. doi:10.1115/SMASIS2020-2261
35. Scholtes D, Schmidt M, Linnebach P, Seelecke S, Motzki P. A multifunctional characterization test bench for shape memory alloy micro-wires—design, implementation and validation. *Mater*. 2023;16(13):4820. doi:10.3390/MA16134820
36. SAES Group. SmartFlex Springs and Wires. https://www.saesgetters.com/sites/default/files/SMARTFLEXSPRINGSANDWIRES.pdf (accessed Jul. 06, 2018)
37. Dynalloy. Technical characteristics of Flexinol actuator wires. Dynalloy Inc. http://www.dynalloy.com/pdfs/TCF1140.pdf (accessed Mar. 12, 2019)
38. Fort Wayne Metals - Nitinol. https://www.fwmetals.com/materials/nitinol/ (accessed May 31, 2023)
39. Auricchio F, Constantinescu A, Menna C, Scalet G. A shakedown analysis of high cycle fatigue of shape memory alloys. *Int J Fatigue*. 2016;87:112-123. doi:10.1016/j.ijfatigue.2016.01.017
40. Scherngell H, Kneissl AC. Generation, development and degradation of the intrinsic two-way shape memory effect in different alloy systems. *Acta Mater*. 2002;50(2):327-341. doi:10.1016/S1359-6454(01)00342-1
41. Muslov SA, Lotkov AI, Timkin VN. Poisson ratio of TiNi. *Inorg Mater Appl Res*. 2022;13(2):306-317. doi:10.1134/S207511332202030
42. Kennedy S, Vlajic N, Perkins E. Cosserat modeling for deformation configuration of shape memory alloy unimorph actuators. *J Intell Mater Syst Struct*. 2023;34(6):642-652. doi:10.1177/1045389X221109256
43. Lalegani Dezaki M, Bodaghi M, Serjouei A, Afazov S, Zolfagharian A. Adaptive reversible composite-based shape memory alloy soft actuators. *Sensors Actuators A Phys*. 2022;345:113779. doi:10.1016/J.SNA.2022.113779
44. Goergen Y, Rizzello G, Motzki P. Systematic methodology for an optimized Design of Shape Memory Alloy-Driven Continuum Robots. *Adv Eng Mater*. 2023;26:2301502. doi:10.1002/ADEM.202301502
45. Kennedy S, Shougat MREU, Perkins E. Robust self-sensing shape memory alloy actuator using a machine learning approach. *Sensors Actuators A Phys*. 2023;354:114255. doi:10.1016/j.sna.2023.114255

SUPPORTING INFORMATION

Additional supporting information can be found online in the Supporting Information section at the end of this article.

How to cite this article: Scholtes D, Seelecke S, Motzki P. Electro-thermo-mechanical characterization of shape memory alloy wires for actuator and sensor applications—Part 1: The effects of training. *Engineering Reports*. 2024;6(10):e12867. doi: 10.1002/eng2.12867